Mean Field Theory of the Lamellar Structure of Block Copolymer/Homopolymer Blends in the Weak Segregation Regime

M. Banaszak and M. D. Whitmore*

Department of Physics, Memorial University of Newfoundland, St. John's, Newfoundland, Canada A1B 3X7

Received September 18, 1991; Revised Manuscript Received January 8, 1992

ABSTRACT: We have studied the lamellar structure of binary A-*b*-B/A and ternary A-*b*-B/A/B copolymer/homopolymer blends near the microphase separation transition. The approach combines perturbative solutions to the modified diffusion equation with a model for the total A and B polymer density profiles. We calculated, approximately, the equilibrium domain and subdomain thicknesses, swelling of the copolymers by the homopolymers, individual polymer density profiles, and their dependence on the copolymer and homopolymer degrees of polymerization, composition, and Flory interaction parameter. The results were compared with numerical solutions to the full self-consistent theory for related copolymer/solvent blends and to three sets of experiments on copolymer/homopolymer blends. The calculations were consistent with the picture that added homopolymers tend to penetrate within the copolymers and swell them laterally and that the degree to which this occurs depends on the relative molecular weights of the copolymers and homopolymers. The tendency of added homopolymers to cause an increase or decrease in the domain thickness correlates with their tendency to stabilize or destabilize the microphase.

1. Introduction

Block copolymers and block copolymer/homopolymer and block copolymer/solvent blends can exhibit a variety of morphologies and phase behavior, undergoing both microphase and macrophase separation. At least four ordered microphases exist: layers, cylinders, spheres, and the interpenetrating "double-diamond" structure.[1,2] The goal of this paper is to provide some additional understanding of the lamellar morphology of such blends near the microphase separation transition (MST), i.e., in the weak segregation regime.

The questions of interest in this paper have been studied experimentally by Quan et al.,[3] Hashimoto et al.,[4-6] and Winey and co-workers.[7] They measured the domain and subdomain thicknesses for series of copolymer/homopolymer blends and extracted the dependence of these quantities on the degrees of polymerization of the homopolymers and the copolymer blocks, blend composition, and temperature. Hashimoto et al. and Winey related their results to the distribution of the added homopolymers within the compatible subdomains and the degree of lateral swelling of the copolymers.

Progress has been made toward a full first-principles treatment of these systems, including the mean field self-consistent theory of Helfand and co-workers for block copolymers in the strong segregation regime,[8-14] Leibler's complementary RPA theory for block copolymers in the weak segregation limit,[15] and its extension to include fluctuation effects by Fredrickson and Helfand.[16] The method of this paper is based on the mean field theory introduced by Hong and Noolandi,[17-19] which has been applied to copolymer/solvent and copolymer/homopolymer blends in the weak and strong segregation regimes.[17-22] For copolymer/solvent blends, the primary application of this approach has employed numerical solutions to the full self-consistent equations of the theory.[17,21] Sufficiently accurate solutions can be particularly difficult to obtain in the weak segregation regime, where the free energy is very small. Hong and Noolandi developed a complementary approach for this regime, employing a perturbative solution to the modified diffusion equations and a resulting fourth-order expansion of the free energy, which has been applied to copolymer/homopolymer and copolymer/solvent blends.[19,20,22]

In this paper we study A-*b*-B/A and A-*b*-B/A/B copolymer/homopolymer blends, using the perturbative solutions to the diffusion equation.[22] We assumed a lamellar structure, restricting attention to systems with overall A:B volume ratios near 50:50, and, using theories of the phase behavior of these systems which were developed earlier and which have been applied to both binary and ternary copolymer/homopolymer blends of this kind, restricted our attention to blends which do not macrophase separate.[19,20,22] We focused on the variation of the lamellar thickness with the copolymer and homopolymer degrees of polymerization and overall volume fractions and on the distribution of copolymers and homopolymers within each subdomain. The approach did not include fluctuation effects or numerical solutions to the self-consistent field equations. The goal was to provide a semiquantitative picture of these systems, leaving for the future a numerical study employing the full self-consistent equations.

In the early work of Hong and Noolandi,[19] as well as other work,[20,22] the fourth-order expansion was combined with the assumption that, near the MST, the density profiles could be modeled by simple cosine-like variations about their mean values. Comparison with numerical self-consistent calculations suggested that this "one-wavenumber approximation" provides a reasonable result for the free energy of the system, but it fails to account for changes in the lamellar thickness with overall concentrations and temperature.[19,21] We have, therefore, incorporated into our approach a model for the density distributions which goes beyond this assumption.

Section 2 of the paper along with the Appendix describes the formalism, including the model for the density distributions. Section 3 begins with a comparison of this approach with numerical self-consistent calculations and goes on to present results for model binary and ternary blends. Section 4 compares the predictions of the theory with measurements made on systems in the strong segregation regime and ends with calculations for some specific blends in the weak segregation regime. Section 5 summarizes.

0024-9297/92/2225-2757$03.00/0

2. Formalism

2.1. General. In this section we summarize the basic expressions used for the equilibrium free energy and density profiles. The method is based on the formalism of ref 22, which is an extension of the work of Hong and Noolandi,[18,19] with incompressibility incorporated followed Ohta and Kawasaki.[23]

We considered a volume V containing $\tilde{N}_c$ copolymer molecules with block degrees of polymerization Z_{cA} and Z_{cB}, $\tilde{N}_{hA}$ homopolymer molecules of type A with degree of polymerization Z_{hA}, and $\tilde{N}_{hB}$ homopolymer molecules of type B with degree of polymerization Z_{hB}. We associated with each component p, p = hA, hB, cA, and cB, a Kuhn statistical length b_p and bulk density ρ_{0p} (monomers per unit volume), and we assumed that the Kuhn lengths and bulk densities of each homopolymer component were the same as those of the corresponding block of the copolymer. The partition function can be written in terms of functional integrals over space curves $\mathbf{r}(\cdot)$ representing polymer molecules. For each homopolymer and each block of a copolymer there is an associated weight function which is assumed to be of the standard Wiener form.

In ref 22 we expressed the partition function as

$$\mathbf{Z} = \mathcal{N}\int [\prod_p d\rho_p(\cdot)\, d\omega_p(\cdot)]\, d\eta(\cdot) \times \exp\{-\mathcal{F}_T[\{\rho_p(\cdot)\},\{\omega_p(\cdot)\},\eta(\cdot)]\} \quad (1)$$

where $\mathcal{F}_T$ is the free energy functional (in units of k_BT) given by

$$\mathcal{F}_T[\{\rho_p(\cdot)\},\{\omega_p(\cdot)\},\eta(\cdot)] = \mathcal{F}[\{\rho_p(\cdot)\},\{\omega_p(\cdot)\}] + \mathcal{G}[\{\rho_p(\cdot)\},\eta(\cdot)] \quad (2)$$

with

$$\mathcal{F}[\{\rho_p(\cdot)\},\{\omega_p(\cdot)\}] = W[\{\rho_p(\cdot)\}] - \sum_p \int d\mathbf{r}\, \omega_p(\mathbf{r})\, \rho_p(\mathbf{r}) + \sum_\kappa^c \tilde{N}_\kappa \left(\ln \frac{\tilde{N}_\kappa}{Z_\kappa \mathcal{Q}_\kappa} - 1 \right) \quad (3)$$

and

$$\mathcal{G}[\{\rho_p(\cdot)\},\eta(\cdot)] = \int d\mathbf{r}\, \eta(\mathbf{r}) \left(\sum_p \frac{\rho_p(\mathbf{r})}{\rho_{0p}} - 1 \right) \quad (4)$$

In these expressions, $W[\{\rho_p(\cdot)\}]$ represents the interaction energy, and the $\mathcal{Q}_\kappa$ can be expressed in terms of four propagators $Q_p(\mathbf{r},\tau|\mathbf{r}')$, all of which satisfy modified diffusion equations.[18] A "c" over a summation sign indicates that the copolymer is to be treated as a single component; otherwise the two blocks are to be treated as distinct.

The thermal average density profile for each component can be expressed

$$\langle \hat{\rho}_p(\mathbf{r}) \rangle = -\frac{\mathcal{N}}{\mathbf{Z}} \int [\prod_{p'} d\rho_{p'}(\cdot)\, d\omega_{p'}(\cdot)]\, d\eta(\cdot)\, \frac{\tilde{N}_\kappa}{\mathcal{Q}_\kappa} \frac{\delta \mathcal{Q}_\kappa}{\delta \omega_p(\mathbf{r})} \times \exp\{-\mathcal{F}_T[\{\rho_{p'}(\cdot)\},\{\omega_{p'}(\cdot)\},\eta(\cdot)]\} \quad (5)$$

where κ = p if p = hA or hB, or κ = c if p = cA or cB.

Evaluation of these functional integrals, without further approximation, is not (yet) possible: in this paper we use the saddle point method. This point was found by minimizing $\mathcal{F}_T$ with respect to each $\rho_p(\mathbf{r})$, $\omega_p(\mathbf{r})$, and $\eta(\mathbf{r})$ subject to the constraint of constant particle numbers. At the saddle point, $\mathcal{G}$ = 0 and hence the saddle point approximation to the free energy is

$$F \to \mathcal{F}[\{\rho_p(\cdot)\},\{\omega_p(\cdot)\}]|_{sp} \quad (6)$$

Similarly, we approximated thermal averages by their values at the saddle point of $\mathcal{F}_T$; eq 5 becomes

$$\langle \hat{\rho}_p(\mathbf{r}) \rangle \to -\frac{\tilde{N}_\kappa}{\mathcal{Q}_\kappa} \frac{\delta \mathcal{Q}_\kappa}{\delta \omega_p(\mathbf{r})}\Big|_{sp} \quad (7)$$

However, since one of the saddle point equations is

$$-\rho_p(\mathbf{r}) - \frac{\tilde{N}_\kappa}{\mathcal{Q}_\kappa} \frac{\delta \mathcal{Q}_\kappa}{\delta \omega_p(\mathbf{r})} = 0 \quad (8)$$

we identified the saddle point value of $\rho_p(\mathbf{r})$ with the saddle point approximation to $\langle \hat{\rho}_p(\mathbf{r}) \rangle$. It should be noted that the derivative acts only on the relevant $\mathcal{Q}_\kappa$, and not on other terms appearing in the free energy.

Assuming that all net A–B interactions are the same, irrespective of whether the interacting monomers belong to homopolymers or copolymers and choosing the overall level of each field $\omega_p(\mathbf{r})$ so that

$$\int d\mathbf{r}\, \omega_p(\mathbf{r}) = 0 \quad (9)$$

then at the saddle point, $\omega_{hA}(\mathbf{r}) = \omega_{cA}(\mathbf{r}) \equiv \omega_A(\mathbf{r})$ and $\omega_{hB}(\mathbf{r}) = \omega_{cB}(\mathbf{r}) \equiv \omega_B(\mathbf{r})$.[22] This agrees with the self-consistent theory of copolymer/solvent blends; if the solvent reference density equals that of the A block of the copolymer, e.g., $\rho_{0S} = \rho_{0A}$, and the interaction parameters are chosen accordingly, i.e., $\chi_{SA} = 0$, $\chi_{AB} = \chi_{SB}$, then the self-consistent potential for the solvent is the same as for the corresponding copolymer block, $\omega_s(\mathbf{r}) = \omega_{cA}(\mathbf{r})$.[18,21] Thus we needed to evaluate the saddle point values of two potentials, $\omega_A(\mathbf{r})$ and $\omega_B(\mathbf{r})$, three $\mathcal{Q}$'s, and derivatives of the $\mathcal{Q}$'s with respect to potentials.

We next rescaled the mean field potentials, Kuhn statistical lengths, and degrees of polymerization:

$$\hat{\omega}_p(\mathbf{r}) = \rho_{0p}\omega_p(\mathbf{r})/\rho_0$$

$$\delta_p^2 = \rho_{0p} b_p^2/\rho_0$$

$$r_{hA} = \rho_0 Z_{hA}/\rho_{0A}, \quad r_{hB} = \rho_0 Z_{hB}/\rho_{0B} \quad (10)$$

$$r_{cA} = \rho_0 Z_{cA}/\rho_{0A}, \quad r_{cB} = \rho_0 Z_{cB}/\rho_{0B}$$

$$r_c = r_{cA} + r_{cB}$$

where ρ_0 is an arbitrary reference density. We also introduced the local and overall average volume fractions of each of the four components

$$\phi_p(\mathbf{r}) = \langle \hat{\rho}_p(\mathbf{r}) \rangle / \rho_{0p} \quad (11)$$

and

$$\bar{\phi}_p = N_p/V\rho_{0p} \quad (12)$$

as well as the overall copolymer volume fraction

$$\bar{\phi}_c = \bar{\phi}_{cA} + \bar{\phi}_{cB} \quad (13)$$

From this point it was convenient to work with Fourier transforms, which we labeled $\tilde{\phi}_p(\mathbf{k})$, $\tilde{\omega}_p(\mathbf{k})$, and $\tilde{Q}_p(\mathbf{k},\tau|\mathbf{k}')$. Using the above results and definitions, the saddle point approximation for the free energy, eq 3, was written as the sum of two parts:

$$F = F_{hom} + \Delta F \quad (14)$$

The first, F_{hom}, is the free energy of a homogeneous bulk

phase of the blend and was discussed in ref 22. The second part, ΔF, is due to inhomogeneities and is what is of direct interest in this paper. Dividing by the volume V and ρ_0, Δf was written

$$\Delta f = \frac{1}{V}\int' \frac{d\mathbf{k}}{(2\pi)^3}\chi\tilde{\phi}_A(\mathbf{k})\,\tilde{\phi}_B(-\mathbf{k}) - \frac{1}{V}\int' \frac{d\mathbf{k}}{(2\pi)^3}\sum_p \tilde{\phi}_p(\mathbf{k})\,\tilde{\omega}_p(-\mathbf{k}) - \sum_\kappa^c \frac{\bar{\phi}_\kappa}{r_\kappa}\ln\frac{\mathcal{Q}_\kappa}{V} \quad (15)$$

Here $U_{AB}\rho_{0A}\rho_{0B}/\rho_0$ was identified with the Flory parameter, χ, describing the net A–B interactions. The local volume fractions of A and B at each point are

$$\phi_A(\mathbf{r}) = \phi_{hA}(\mathbf{r}) + \phi_{cA}(\mathbf{r}) \quad (16)$$

and

$$\phi_B(\mathbf{r}) = \phi_{hB}(\mathbf{r}) + \phi_{cB}(\mathbf{r}) \quad (17)$$

which, because of incompressibility, satisfy $\phi_A(\mathbf{r}) + \phi_B(\mathbf{r}) = 1$. In Fourier space they satisfy

$$\tilde{\phi}_B(\mathbf{k}) = -\tilde{\phi}_A(\mathbf{k}) \quad \text{for } \mathbf{k} \neq 0 \quad (18)$$

The average volume fractions of A and B in the system are denoted $\bar{\phi}_A$ and $\bar{\phi}_B$. The "prime" on the integration symbol in eq 15 means to exclude $\mathbf{k} = 0$.

The formalism has now been transformed so that the perturbative solutions to the diffusion equation can be used directly.[19] For any potential $\tilde{\omega}_p$, $\tilde{Q}_p(\mathbf{k},\tau|\mathbf{k}')$ can be given as an expansion in the $\tilde{\omega}_p$, which can then be integrated to evaluate the $\mathcal{Q}_\kappa$. For κ = hA, hB, or c, this yields

$$\frac{\mathcal{Q}_\kappa}{V} = 1 + \frac{(-r_\kappa)^2}{2!V}g^\kappa_{ij}\tilde{\omega}_i\tilde{\omega}_j + \frac{(-r_\kappa)^3}{3!V}g^\kappa_{ijk}\tilde{\omega}_i\tilde{\omega}_j\tilde{\omega}_k + \frac{(-r_\kappa)^4}{4!V}g^\kappa_{ijkl}\tilde{\omega}_i\tilde{\omega}_j\tilde{\omega}_k\tilde{\omega}_l + \dots \quad (19)$$

where $i \equiv (i,\mathbf{k}_i)$, $\tilde{\omega}_i = \tilde{\omega}_i(-\mathbf{k})$, and summation over subscript and integration over wavevector are implied by repeated indices. In these summations, i, j, ... = hA, hB, cA, or cB, and we use $\omega_{hA} = \omega_{cA} = \omega_A$, etc. The functions $g^\kappa_{ij\dots l}$ are given in ref 19. The use of this expansion restricted the range of validity of the approach to regions where the ω_p and Δf are in some sense small, i.e., the weak segregation regime.

We used eq 19 in two ways. First, we used it directly in eq 15 to express Δf (at the saddle point) as

$$\Delta f = \frac{1}{V}\int' \frac{d\mathbf{k}}{(2\pi)^3}\chi\tilde{\phi}_A(\mathbf{k})\,\tilde{\phi}_B(\mathbf{k}) - \frac{1}{V}\int' \frac{d\mathbf{k}}{(2\pi)^3}[\tilde{\phi}_A(\mathbf{k})\,\tilde{\omega}_A(-\mathbf{k}) + \tilde{\phi}_B(\mathbf{k})\,\tilde{\omega}_B(-\mathbf{k})] - \frac{1}{2V}\mathcal{G}_{ij}\tilde{\omega}_i\tilde{\omega}_j + \frac{1}{6V}\mathcal{G}_{ijk}\tilde{\omega}_i\tilde{\omega}_j\tilde{\omega}_k - \frac{1}{24V}\mathcal{G}_{ijkl}\tilde{\omega}_i\tilde{\omega}_j\tilde{\omega}_k\tilde{\omega}_l + \dots \quad (20)$$

with the coefficients given in ref 22. Second, since eq 19 is valid for any value of the potential, not just the saddle point values, we can differentiate it and then evaluate these derivatives at the saddle point. Differentiating $\mathcal{Q}_c$ with respect to $\tilde{\omega}_A$ or $\tilde{\omega}_B$ gave

$$\tilde{\phi}_p(\mathbf{k}) = -r_c\bar{\phi}_c g^c_{pj}\tilde{\omega}_j + \frac{1}{2}r_c^2\bar{\phi}_c g^c_{pjk}\tilde{\omega}_j\tilde{\omega}_k - \frac{1}{6}r_c^3\bar{\phi}_c\left(g^c_{pjkl} - \frac{3}{V}g^c_{pj}g^c_{kl}\right)\tilde{\omega}_j\tilde{\omega}_k\tilde{\omega}_l + \dots \quad (21)$$

for p = cA or cB. Differentiating $\mathcal{Q}_{hA}$ with respect to $\tilde{\omega}_A$ or $\mathcal{Q}_{hB}$ with respect to $\tilde{\omega}_B$ gave

$$\tilde{\phi}_p(\mathbf{k}) = -r_p\bar{\phi}_p g^p_{pj}\tilde{\omega}_j + \frac{1}{2}r_p^2\bar{\phi}_p g^p_{pjk}\tilde{\omega}_j\tilde{\omega}_k - \frac{1}{6}r_p^3\bar{\phi}_p\left(g^p_{pjkl} - \frac{3}{V}g^p_{pj}g^p_{kl}\right)\tilde{\omega}_j\tilde{\omega}_k\tilde{\omega}_l + \dots \quad (22)$$

for p = hA or hB. Adding pairs of these expressions as indicated in eqs 16 and 17 yielded, for $\mathbf{k} \neq 0$

$$\tilde{\phi}_i(\mathbf{k}) \simeq \mathcal{G}_{ij}\tilde{\omega}_j + {}^1/_2\mathcal{G}_{ijk}\tilde{\omega}_j\tilde{\omega}_k - {}^1/_6\mathcal{G}_{ijkl}\tilde{\omega}_j\tilde{\omega}_k\tilde{\omega}_l \quad (23)$$

for i, j, k, l = A or B, and the $\mathcal{G}$'s are the same as in eq 20. Inverting this yields $\tilde{\omega}_A$ and $\tilde{\omega}_B$ in terms of $\tilde{\phi}_A$ and $\tilde{\phi}_B$, which for $\mathbf{k} \neq 0$ up to the third order is

$$\tilde{\omega}_i(\mathbf{k}) \simeq \Gamma^2_{ij}\tilde{\phi}_j + \Gamma^3_{ijk}\tilde{\phi}_j\tilde{\phi}_k + \Gamma^4_{ijkl}\tilde{\phi}_j\tilde{\phi}_k\tilde{\phi}_l \quad (24)$$

where the Γ's are given in ref 22. Substituting eq 24 into eq 20 and using eq 18 yields

$$\Delta f \simeq \sum_{\mathbf{k}_1}' f^{(2)}(\mathbf{k}_1,-\mathbf{k}_1)\,\tilde{\phi}_A(\mathbf{k}_1)\,\tilde{\phi}_A(-\mathbf{k}_1) + \sum_{\mathbf{k}_1,\mathbf{k}_2}' f^{(3)}(\mathbf{k}_1,\mathbf{k}_2,-\mathbf{k}_1-\mathbf{k}_2)\,\tilde{\phi}_A(\mathbf{k}_1)\,\tilde{\phi}_A(\mathbf{k}_2)\,\tilde{\phi}_A(-\mathbf{k}_1-\mathbf{k}_2) + \sum_{\mathbf{k}_1,\mathbf{k}_2,\mathbf{k}_3}' f^{(4)}(\mathbf{k}_1,\mathbf{k}_2,\mathbf{k}_3,-\mathbf{k}_1-\mathbf{k}_2-\mathbf{k}_3)\,\tilde{\phi}_A(\mathbf{k}_1)\,\tilde{\phi}_A(\mathbf{k}_2)\times\tilde{\phi}_A(\mathbf{k}_3)\,\tilde{\phi}_A(-\mathbf{k}_1-\mathbf{k}_2-\mathbf{k}_3) \quad (25)$$

where the prime on the sums means to exclude $\mathbf{k}_i = 0$. The coefficients $f^{(2)}$, $f^{(3)}$, and $f^{(4)}$ are listed in ref 22.

This provided, in principle, a prescription for calculating Δf and the four density profiles (in the weak segregation regime). The first step was to calculate the $\tilde{\phi}_A(\mathbf{k})$ by minimizing Δf, i.e., eq 25. Then using $\tilde{\phi}_B(\mathbf{k}) = -\tilde{\phi}_A(\mathbf{k})$, the two fields ω_A and ω_B were calculated from eq 24. From these the four individual density profiles were calculated from eqs 21 and 22. Because of the inversion of eq 23 and minimization of a truncated series for Δf, in order to maintain a consistent level of approximation, at this last step we truncated eqs 21 and 22 to second order. For example, eq 21 was evaluated as

$$\tilde{\phi}_p(\mathbf{k}) \simeq -r_c\bar{\phi}_c g^c_{pj}\tilde{\omega}_j + {}^1/_2r_c^2\bar{\phi}_c g^c_{pjk}\tilde{\omega}_j\tilde{\omega}_k \quad (26)$$

2.2. Model Density Profiles. In principle, we needed to minimize Δf with respect to all the $\tilde{\phi}_A(\mathbf{k})$. In practice, we considered a restricted family of possible $\tilde{\phi}_A(\mathbf{k})$, in order to carry out the minimization in a numerically efficient way. This family was chosen on the basis of a number of considerations. First, we assumed that $\phi_A(x)$ monotonically decreases from the center of one subdomain to the center of the other one, and we required that its value lie between zero and unity everywhere. Second, the family of functions must include the possibility that the spatial dependence of $\phi_A(x)$ is simply a cosine variation about its average value; i.e., $\phi_A(x)$ approaches

$$\phi_A(x) \to \bar{\phi}_A + \Psi_A\cos(k^*x) \quad (27)$$

where $k^* = 2\pi/d$, with d being the lamellar thickness, and Ψ_A is the amplitude of the variation. This is the form expected in mean field theory as the system approaches the MST (for the lamellar structure). In this limit, $\phi_B(x)$ has the same form with an associated prefactor $\Psi_B = -\Psi_A$. Third, the family must be able to model the expected changes in $\phi_A(x)$ as the system parameters evolve toward the stronger segregation regime, i.e., increased magnitudes of Ψ_A and Ψ_B, unequal subdomain thicknesses, unequal function values within each subdomain, plateaus in the profiles within each subdomain, and narrowed interphase regions.

In our calculations, we represented $\phi_A(x)$ by a family of functions with the flexibility to satisfy these conditions. We used

$$\phi_A(x) = \bar{\phi}_A + \Psi_A\, u(x;d,\sigma,\tau) \tag{28}$$

where d is the repeat distance and σ and τ are two variables which control the shape of $\phi_A(x)$. The functional form chosen for $u(x)$ is discussed in the Appendix. For one limiting set of values of σ and τ, $u(x)$ reduces to a single cosine function, as in eq 27. As these two parameters are changed, the profiles change, eventually reaching the other limiting case in which $\phi_A(x) = 1$ throughout the most of one subdomain, $\phi_A(x) = 0$ throughout most of the other, and $\phi_A(x)$ is given by a hyperbolic tangent in the interphase. This would be the expected profile for copolymers in the strong segregation limit.[14]

Substituting eq 28 into eq 25 provided an expression for Δf which was a function of the four variables Ψ_A, d, σ, and τ. For any values of these, we evaluated the multiple sums appearing in eq 25. Minimizing this function with respect to these variables gave the calculated equilibrium layer thickness d and density profile $\tilde{\phi}_A$. From this we calculated $\tilde{\phi}_B = -\tilde{\phi}_A$, the two potentials ω_A and ω_B from eq 24, and then the four $\tilde{\phi}_p$ from eqs 21 and 22.

Having completed such a calculation, we converted the results to real space and finished by verifying that the solution which was obtained was physically acceptable, i.e., that all four local volume fractions $\phi_p(x)$ remained between 0 and 1 everywhere. This restriction limited the calculations to near the MST, and the calculted profiles never reached the hyperbolic tangent shape. For all such cases, we found that keeping 12 wavenumbers in the summations kept the truncation error to the order of 10^{-14}.

Finally, we identified the point of inflection in $\phi_A(x)$ as the point which divides d into the two subdomains, of thicknesses d_A and d_B.

3. Model Calculations

3.1. Comparison with Self-Consistent Calculations. In this section, we examine a model system in which all reference densities and Kuhn lengths were equal and, for purposes of illustration, chose the copolymer degree of polymerization to be $Z_c = 400$ as in our earlier work.[22] This value is also close to that for the copolymers in the work of Hashimoto et al.[4-6] In most of the cases we exhibit, all homopolymers were assumed to have the same degree of polymerization, in which case we simplify the notation by relabeling them $Z_{hA} = Z_{hB} \equiv Z_h$.

We begin by comparing results using the approach described above with results obtained from the full mean field self-consistent theory for binary copolymer/solvent blends. For this comparison we used symmetric copolymers, i.e., $Z_{cA} = Z_{cB} = Z_c/2$, and chose the interaction parameters to be $\chi_{SB} = \chi_{AB} = \chi$ and $\chi_{SA} = 0$. Within the approximate approach, the solvent was represented as an hA homopolymer with $Z_h = 1$. This comparison was meant to test the combination of the fourth-order free energy expansion with the model density profile, i.e., eq 28 with $u(x;d,\sigma,\tau)$ as described, near the MST. It did not test mean field theory itself, nor did it necessarily represent a realistic model of a real system. For example, the polystyrene–styrene interaction parameter has been determined to be close to 0.5, not zero.[24] As well, we did not investigate here the possibility of the other morphologies being stable very near the order–disorder transition.

The self-consistent calculations were carried out as described in refs 17 and 21, but with the parameter describing the range of the potential, labeled σ in those references, set to zero. Near the MST where the free energy Δf approached zero, the required accuracy in the self-consistent solutions to the diffusion equation and resulting density profiles was on the order of 6 significant figures.

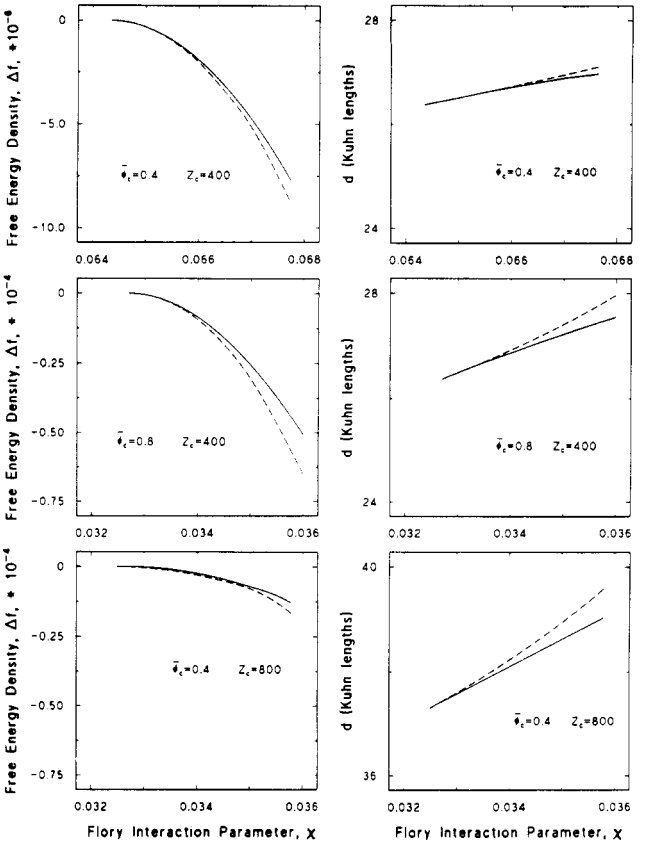

Figure 1. Comparison of self-consistent calculations and approximate method: equilibrium free energy (left-hand column) and domain thickness (right-hand column) for three cases, as indicated. The solid lines are the results of numerical solutions to the full self-consistent equations, and the dashed lines were calculated using the method based on the fourth-order expansion, with $Z_h = 1$.

Three series of calculations are shown. In two of them, $Z_c = 400$ and $\bar{\phi}_c = 0.4$ (series 1) or 0.8 (series 2). For the third, $\bar{\phi}_c = 0.4$ as in the first series, but Z_c was increased to 800. The first and second columns of Figure 1 show, respectively, the free energy Δf and the domain thickness d as a function of χ for the three systems calculated both ways. At least to within the numerical accuracy, in both methods the free energy vanished with zero derivative at values of χ which agreed to 3 significant figures, and Δf and d agreed as the MST is approached. As χ increased, the self-consistent calculations gave a slightly higher value of Δf, a difference attributable to the truncation of the expansion. As seen in the second column, both calculations predicted an increase in d with χ, with the approximate calculation predicting a slightly faster increase. The difference virtually vanished near, but not soley at, the MST. If, as is customary, we express the dependence of d on χ as $d \propto \chi^p$, then for all three systems shown, very close to the MST, the self-consistent calculations gave $p = 0.50 \pm 0.01$ and the approximate method gave $p = 0.51 \pm 0.01$. This contrasts with the one wavenumber approximation in which d is independent of χ.

Figure 2 shows calculated density profiles for each blend of Figure 1. For each case, we have chosen the largest value of χ used in the corresponding panel of Figure 1, where the difference between the two sets of calculations was the largest. The left-hand column of Figure 2 shows

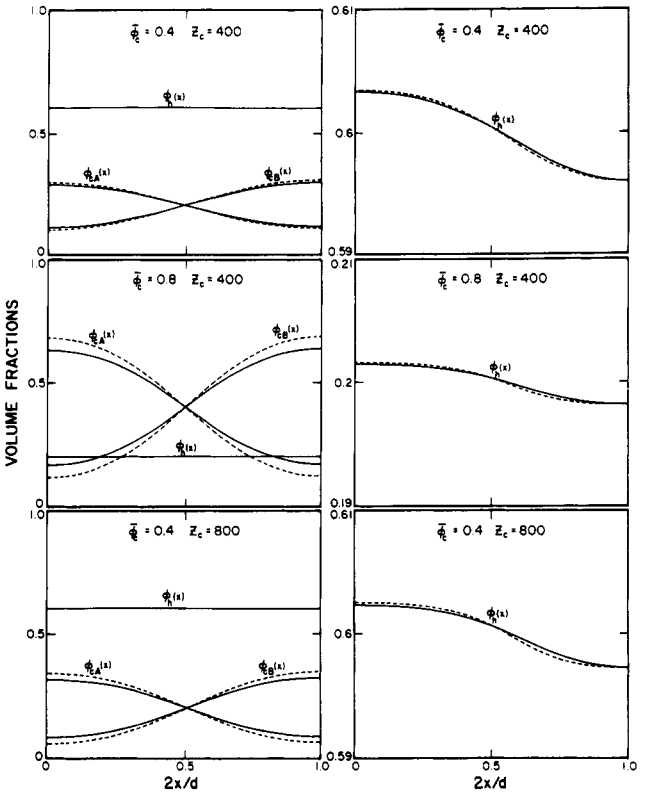

Figure 2. Comparison of self-consistent calculations and approximate method: local volume fractions $\phi_{cA}(x)$, $\phi_{cB}(x)$, and $\phi_h(x)$ for the three cases of Figure 1. The solid lines are the results of numerical solutions to the full self-consistent equations, and the dashed lines were calculated using the method based on the fourth-order expansion, with $Z_h = 1$. The panels in the right-hand column show the solvent density profiles on an expanded scale. For purposes of illustration, the horizontal axis is normalized to $d/2$.

the three density profiles for each system, $\phi_{cA}(x)$ and $\phi_{cB}(x)$ for the copolymer components and $\phi_h(x)$ for the solvent. The right-hand side reproduces $\phi_h(x)$ on a greatly expanded scale. Qualitatively, the two approaches gave the same results, with very similar shapes for each set of density profiles. Quantitatively, the fourth-order expansion overestimated the amplitude of the variations of $\phi_{cA}(x)$ and $\phi_{cB}(x)$ by about 10–25%. In all cases the density variation of the solvent, $\psi_h(x)$, was very small, and the two approaches predicted almost identical profiles.

3.2. Domain and Subdomain Thicknesses. Figure 3 shows the first series of calculations for model binary copolymer/homopolymer blends with $Z_c = 400$ and different homopolymer degrees of polymerization, with Z_h varying from 1 to 120. As in most of the experiments discussed in section 4,[3-7] we considered homopolymer volume fractions up to $\bar{\phi}_h = 0.2$, which for the case of symmetric copolymers corresponds to an overall A:B composition ratio of 60:40. Over at least most of this range, we expect the lamellar morphology to be the equilibrium structure.[2] As well, we chose $\chi = 0.03$, so that for the pure copolymer $\chi Z_c = 12$, which placed the system near but not at the MST.

Figure 3 shows the calculated changes in d, d_A, and d_B resulting from the addition of the homopolymers. Beginning with the lamellar thickness d, the top panel shows that for "small" Z_h, d decreased, but for larger Z_h, it increased. The curve for $Z_h = 1$ terminates at $\bar{\phi}_c = 0.87$, because this is the MST for this system. There was a threshold value of Z_h, say Z_h^{th}, such that if $Z_h = Z_h^{th}$, then small amounts of homopolymer induced no change in d.

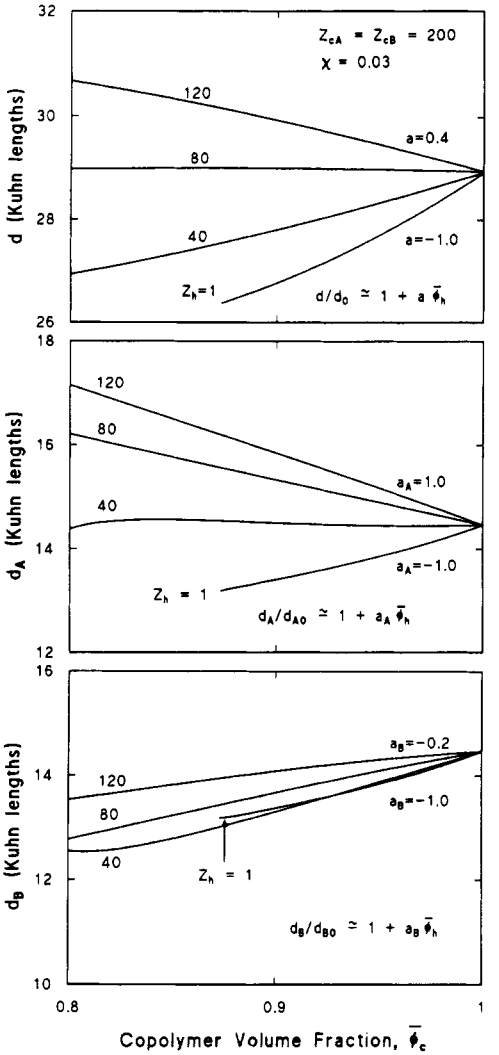

Figure 3. Equilibrium domain thickness d (upper panel) and subdomain thicknesses d_A and d_B (middle and lower panels) as functions of copolymer content $\bar{\phi}_c$ for the model binary blend with $Z_{cA} = Z_{cB} = 200$ for different degrees of polymerization of the added homopolymer, Z_h, as indicated. The curves for $Z_h = 1$ terminate at $\bar{\phi}_c = 0.87$, corresponding to the MST.

Table I
Initial Dependence of the Domain Thickness d and Subdomain Thicknesses d_A and d_B on Small Amounts of Homopolymer for Binary A-*b*-B/A and Ternary A-*b*-B/A/B Blends[a]

			binary blends			ternary blends		
Z_c	Z_{cA}/Z_c	Z_h	a	a_A	a_B	a	a_A	a_B
400	0.5	1	−1.0	−1.0	−1.0	−1.0	−1.0	−1.0
		120	0.4	1.0	−0.2	0.4	0.4	0.4
	0.4	1	−0.6	−0.3	−0.8	−0.6	−0.4	−0.8
		120	0.9	1.5	0.5	0.4	0.3	0.5

[a] For all cases, $\chi = 0.03$. For the ternary blends, the homopolymers have equal degrees of polymerization, $Z_{hA} = Z_{hB} \equiv Z_h$, and they are added in a proportion to maintain the blends on the isopleth. The coefficients a, a_A, and a_B are defined by eqs 30, 33, and 34.

The precise value Z_h^{th} depends on what is meant by "small", but it is clear that it is about

$$Z_h^{th} \simeq Z_c/5 \tag{29}$$

For very small amounts of homopolymer, the changes in d can be expressed

$$d/d_0 \simeq 1 + a\bar{\phi}_h \tag{30}$$

where $\bar{\phi}_h$ is the overall homopolymer volume fraction, which for these binary blends is $\bar{\phi}_h = \bar{\phi}_{hA}$, and d_0 is the

layer thickness for the pure copolymer. The values of a ranged from about −1.0 for small Z_h to about +0.4 for $Z_h = 0.3Z_c$. These values, as well as related ones for other model systems, are summarized in Table I.

This behavior, including the existence of the threshold, differed qualitatively from what is predicted by the one-wavenumber approximation. In that approach, d is determined by minimizing the second-order term in the free energy. For small $\bar{\phi}_h$, it predicts

$$\frac{d}{d_0} \simeq 1 + 2\bar{\phi}_h\left(\frac{Z_h}{Z_c}\right)^2 \frac{g_h'(2Z_h x_0^*/Z_c)}{x_0^* g_c''(x_0^*)} \tag{31}$$

where

$$g_h(x) = g_h^{(2)}(x)$$

$$g_c(x) = g_{cA}^{(2)}(x) - [g_{cA}^{(1)}(x)]^2 \tag{32}$$

and $g_h^{(2)}$, $g_{cA}^{(2)}$, and $g_{cA}^{(1)}$, which are directly related to the $g_{i,j}^{\kappa}$, were defined in ref 19. The primes denote derivatives, with x_0^* which denotes the location of the maximum of g_c, has the value $x_0^* = 22.7/12$. It is related to d_0 by $x_0^* = Z_c b^2[k^*]^2/12$, with $d_0 = 2\pi/k^*$. There are three points to note. First this approach always underestimates d, giving the value appropriate for the MST. Second, since x_0^* corresponds to the maximum in g_c and since g_h is monotonically decreasing, the combination g_h'/g_c'' is always positive, and so this approach implies that added homopolymers would always induce an increase in d. Finally, however, the size of the increase depends on the ratio Z_h/Z_c, and since this vanishes for small Z_h, in particular for solvent, d becomes virtually independent of $\bar{\phi}_h$ in this limit.

The prediction of the one-wavenumber approximation that added solvent induces virtually no change in the layer thickness is similar to an earlier comment by Hong and Noolandi that for *neutral* solvent this approximation leads to the prediction that d is independent of solvent concentration.[19] They pointed out that the higher order effects lead to a reduction in d with added solvent.[21]

We can understand the behavior of d, and, in particular, the relationship between the one-wavenumber results and the current results in the following way. The first point to note is that, for these copolymers, at the MST the repeat distance would be $d_0/b \simeq 26.4$, i.e., the one-wavenumber value. However, for the chosen value of χ, $\chi Z_c = 12$, and hence d_0 is larger, $d_0/b \simeq 29$. Second, recall that induced microphase formation was predicted to occur for this blend if $Z_h \gtrsim Z_c/4$.[20] This implies that addition of lower molecular weight homopolymers drives the system toward the weak segregation regime, the density profiles tend toward simple cosine functions, and d relaxes downward toward its MST value. For the case shown in Figure 3 which reaches the order–disorder transition, $Z_h = 1$, the value of d at the transition is just that predicted by the one-wavenumber approximation. Conversely, adding higher molecular weight homopolymers at least initially drives the system toward the strong segregation regime, which of itself would induce a further increase in d. Thus the tendency to stabilize or destabilize the microphase is correlated with the tendency to cause d to increase or decrease. This picture, as well as other results such as the values of the threshold Z_h^{th} and the coefficient a (and a_A and a_B defined below), very likely depends on where the system is in terms of the weak or strong segregation regimes.

Returning now to Figure 3, the subdomain thicknesses d_A and d_B for this system are illustrated in the two lower panels. The initial behavior of d_A resembled that of d, except that, for a given Z_h, the increase in d_A was greater than the increase in d, and d_A increased for all $Z_h \gtrsim 40$. This compares with the threshold value for d for this system of $Z_h^{th} \simeq 80$. By contrast, in all cases, d_B initially decreased as A homopolymers are added. Expressing these initial changes in d_A and d_B as in eq 30

$$d_A/d_{A0} \simeq 1 + a_A\bar{\phi}_h \tag{33}$$

and

$$d_B/d_{B0} \simeq 1 + a_B\bar{\phi}_h \tag{34}$$

we found the initial slope range from $a_A = a_B \simeq -1.0$ for $Z_h = 1$ to $a_A \simeq 1.0$ and $a_B \simeq -0.2$ for $Z_h = 120$.

For larger homopolymer concentrations, the changes in d_A and d_B were more complex, reflecting three effects. First, the overall increase in $\bar{\phi}_A$ tended to induce an increase in d_A. Second, in general, the added homopolymers tended to drive the system toward either the weak or the strong segregation regimes, tending to induce a decrease or an increase in d, respectively. Finally, as a system approached the MST, both d_A and d_B tended toward $d/2$. The case $Z_h = 40$ illustrates these. For d_A, there was initially a balance of the first two effects, and it was nearly constant for homopolymer content up to $\bar{\phi}_h \simeq 0.17$, at which point it began to decrease toward $d/2$ as the system approached the MST. On the other hand, d_B initially decreased, reaching a minimum near $\bar{\phi}_h \simeq 0.17$, after which it increased slightly. For $Z_h = 1$, the system reached the MST at $\bar{\phi}_c = 0.87$, where $d_A = d_B = d/2$.

We next considered one example with asymmetric copolymers, chosen to have $Z_c = 400$ as above, but $Z_{cA} = 160$ and $Z_{cB} = 240$, so the overall composition ratio was $\bar{\phi}_A:\bar{\phi}_B = 40:60$. The addition of 20% homopolymer A changed this ratio to 52:48, and so once again the morphology would probably remain lamellar throughout this range. Figure 4, which is analogous to Figure 3, shows d, d_A, and d_B as functions of $\bar{\phi}_c$ for this case. For this system, the curves for $Z_h = 1$ and $Z_h = 40$ both terminate where the blends reach the MST. For the case $Z_h = 120$, we terminated the calculations at $\bar{\phi}_c = 0.85$, because beyond this the calculated density distributions became unphysical, as described in section 2. We indicate this by extrapolating with a dotted line.

Considering d first, in all cases its increase was greater than for the corresponding case with the symmetric copolymers. Consistent with this, there was again a threshold value of Z_h such that for larger (smaller) Z_h, the overall repeat distance d increased (decreased), but in this case it was at $Z_h^{th} \simeq 45 \simeq Z_c/9 \simeq Z_{cA}/3.5$, which compares with $Z_h^{th} \simeq Z_c/5 \simeq Z_{cA}/2.5$ found above for the symmetric copolymer case.

The variations of d_A and d_B were particularly interesting. For neat copolymer, $d_A \simeq 11.5 < d/2$ and $d_B \simeq 13.5 > d/2$. As very low molecular weight homopolymers were added, the system moved toward the MST, d decreased, and both d_A and d_B initially followed; e.g., for $Z_h = 1$, $a \simeq -0.6$, $a_A \simeq -0.3$, and $a_B \simeq -0.8$. However, with the addition of only small amounts of these homopolymers, the tendency for d_A and d_B to change toward $d/2$ dominated, causing d_A to increase and d_B to decrease rapidly. For the higher molecular weight homopolymers, e.g., $Z_h = 120$, both d_A and d_B increased, in contrast with corresponding behavior for the symmetric copolymer/homopolymer blends, in which d_B decreased.

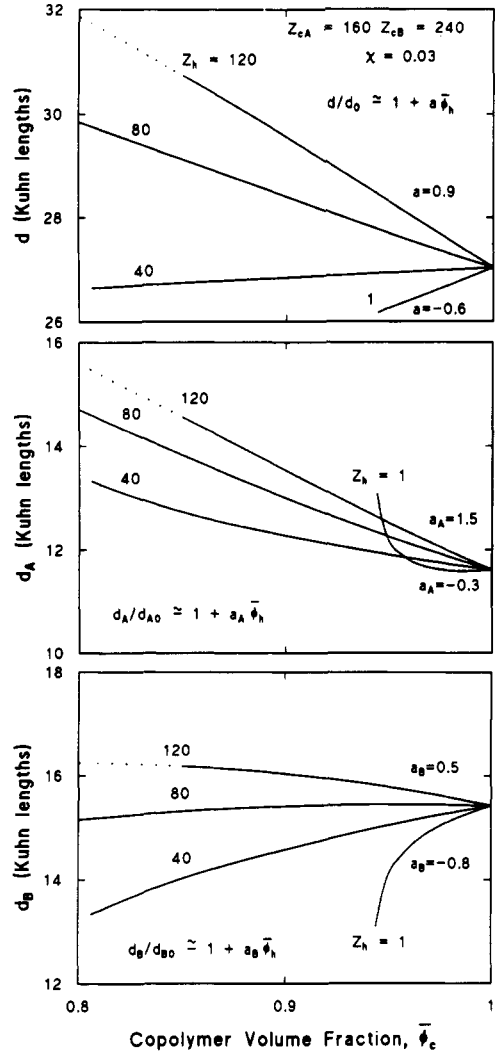

Figure 4. Equilibrium domain thickness d and subdomain thicknesses d_A and d_B as functions of $\bar{\phi}_c$ for the model binary blend with asymmetric copolymers for different degrees of polymerization of the added homopolymer, Z_h, as indicated. The curves for Z_h = 1 and 40 terminate at ϕ_c = 0.94 and 0.81, respectively, corresponding to the MST in each case. For Z_h = 120, the dotted lines are extrapolations of the calculations to $\bar{\phi}_c$ < 0.85, where the method gives unphysical densities.

Turning to ternary blends, we begin with model systems with symmetric copolymers blended with equal amounts of A and B homopolymers with equal degrees of polymerization, i.e., $\bar{\phi}_{hA} = \bar{\phi}_{hB} = \bar{\phi}_h/2$ and $Z_{hA} = Z_{hB} \equiv Z_h$. This simplifies the results, because $d_A = d_B = d/2$. Figure 5, which is analogous to the upper panel of Figure 3, shows calculated values of d for such blends with Z_c = 400 and Z_h varying from 1 to 120. For small Z_h, the behavior of d was virtually identical to that for the binary blends. For larger Z_h, it was almost the same for very low $\bar{\phi}_h$, reflected in the fact that the values of the coefficient a were the same in corresponding cases, and furthermore in this limit the threshold value of Z_h remained the same, $Z_h^{th} \simeq Z_c/5$. However, as $\bar{\phi}_h$ was increased, there were quantitative differences. Finite concentrations of homopolymer, e.g., 10–20%, tended to induce a larger increase in d than in the binary case; for example, for Z_h = 120, the increase in d at $\bar{\phi}_c$ = 0.8 was about 50% larger. Another (obvious) difference from the binary blends in this case was that $d_A = d_B = d/2$.

For the final model system, we considered ternary blends with the same asymmetric copolymers as in Figure 4,

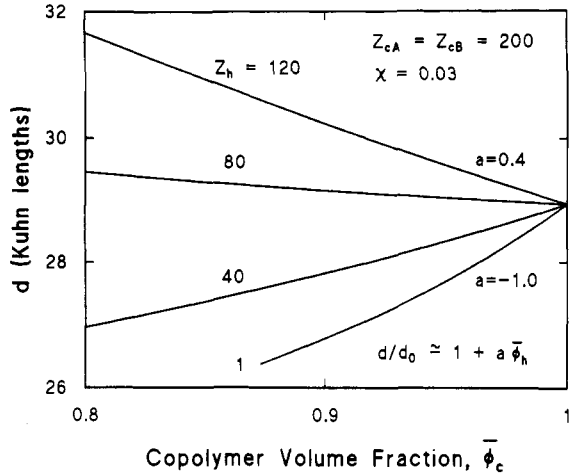

Figure 5. Equilibrium domain thickness d as a function of $\bar{\phi}_c$ for model ternary blends with $Z_{cA} = Z_{cB}$ = 200 for different degrees of polymerization of the added homopolymer, Z_h, as indicated. The systems are on the isopleth, so $d_A = d_B = d/2$. The curve for Z_h = 1 terminates at $\bar{\phi}_c$ = 0.873, corresponding to the MST.

blended with A and B homopolymers with equal degrees of polymerization but added in a proportion to maintain the system on the isopleth; i.e., the overall volume fractions remained $\bar{\phi}_A$:$\bar{\phi}_B$ = 40:60. Figure 6 shows d, d_A, and d_B as a function of $\bar{\phi}_c$ for this case. As for the cases using symmetric copolymers, the results for binary and these ternary blends were almost identical for Z_h = 1. However, the differences for larger Z_h were more pronounced, reflecting in part the fact that the overall A:B concentration remained 40:60, and the MST was reached at higher $\bar{\phi}_c$. In general, the decrease in d was faster, or its increase was slower, and the threshold (for the limit $\bar{\phi}_h \to 0$) was increased by about 50% to $Z_h^{th} \simeq 70 \simeq Z_c/6$. For Z_h = 40, because the MST was reached sooner in the ternary blends, the rapid changes in d_A and d_B (toward d/2) occurred at large $\bar{\phi}_c$. For larger Z_h and the volume fractions shown, the increases in d_A were smaller but the tendency for d_B to increase was larger in the ternary blends compared with the binary blends.

Figure 7 shows the calculated variation of d with the interaction parameter χ for the binary systems modeled above with the symmetric copolymers. The results for ternary blends were almost identical, and so are not shown. In all cases we restricted attention to the region very near the MST, with each line terminating at the value of χ corresponding to the MST. Referring back to the results shown in Figure 1, it is probable that the variation in d was well represented by our model over this range of χ (to the extent that mean field theory is adequate).

The calculations show a number of effects, at least qualitatively. First, expressing the results again as $d \propto \chi^p$, for the pure copolymer we found $p \simeq 0.5$, as above. Second, as solvent was added, the transition was shifted to higher values of χ, for a given χ the value of d decreased, and the value of p remained very near 0.5. For Z_h = 40, the transition remained shifted to higher values of χ and for a given χ the value of d was again decreased. However, the dependence of d on χ strengthened slightly as homopolymers were added; p increased to almost 0.6 at $\bar{\phi}_c$ = 0.8. Finally, for $Z_h = Z_c/4$, the transition was nearly unshifted, for a given χ the value of d was increased, and the dependence of d on χ further increased slightly with p = 0.6 at $\bar{\phi}_c$ = 0.8 in the binary blend, and p slightly greater than 0.6 in the ternary blend.

3.3. Homopolymer Localization and Density Profiles. We next turn to relating the above results to

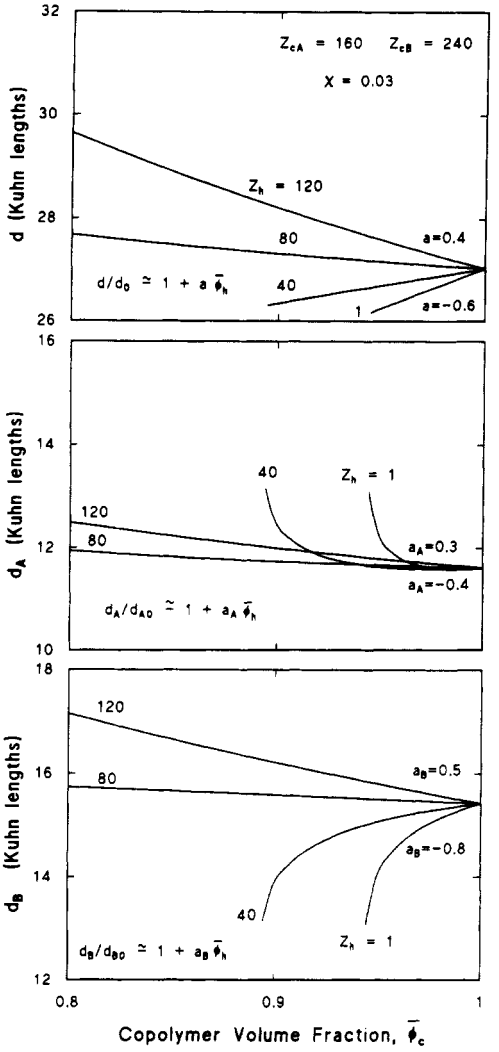

Figure 6. Equilibrium domain and subdomain thicknesses, d, d_A, and d_B, as functions of $\bar{\phi}_c$ for model ternary blends with asymmetric copolymers. In each case, $Z_{hA} = Z_{hB} \equiv Z_h$, with values as indicated. The systems are on the isopleth, maintaining a constant overall ratio $\bar{\phi}_A:\bar{\phi}_B$ = 2:3. The curves for Z_h = 1 and 40 terminate at $\bar{\phi}_c$ = 0.944 and 0.895, respectively, the MST in each case.

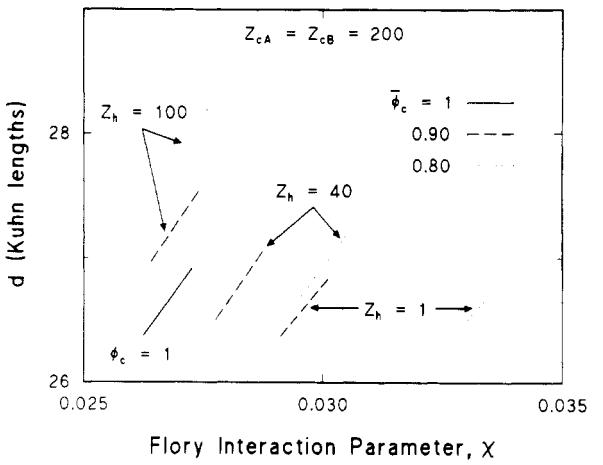

Figure 7. Equilibrium domain thickness d as a function of interaction parameter χ for binary blends with symmetric copolymers. The solid line represents pure copolymer, dashed lines represent blends with $\bar{\phi}_c$ = 0.9, and the dotted lines represent blends with $\bar{\phi}_c$ = 0.8. Results are shown for three different homopolymer degrees of polymerization, Z_h, as indicated.

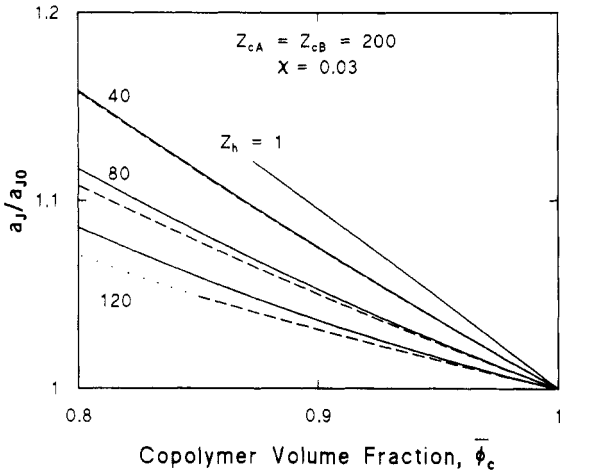

Figure 8. Square root of the average cross-sectional area per copolymer molecule in each interface, a_J, relative to its value for the neat copolymer system, a_{J0}, as a function of $\bar{\phi}_c$ for the systems with symmetric copolymers. The solid curves correspond to binary blends, as in Figure 3, and the dashed curves correspond to ternary blends on the isopleth as in Figure 5.

the distribution of each component within the domains and subdomains. Following Tanaka et al.,[5] we begin by considering the square root of the average cross-sectional area per copolymer molecule in each domain, a_J. (In the strong segregation regime, a_J is proportional to the average nearest-neighbor distance between joints.) The degree to which a_J increases as solvent or homopolymers are added indicates the degree to which the added molecules penetrate within the copolymers and swell the system laterally. If added solvent penetrates both subdomains, then both d_A and d_B decrease. On the other hand, if hA is preferentially solubilized in the A domain, e.g., in binary blends, then d_A increases but the induced lateral swelling of the copolymers causes d_B to decrease. If added homopolymers are solubilized in both domains, e.g., in ternary blends, then d_A and d_B can either increase or decrease.

Changes in a_J are quantitatively related to changes in $\bar{\phi}_c$ and d by

$$\frac{a_J}{a_{J0}} = \left[\frac{d_0}{d\bar{\phi}_c}\right]^{1/2} \tag{35}$$

For low homopolymer concentrations, these variations are simply related. Substituting eq 30 into eq 35 and expanding yields

$$\frac{a_J}{a_{J0}} \simeq 1 + \left(\frac{1-a}{2}\right)\bar{\phi}_h \tag{36}$$

where a is the coefficient appearing in eq 30. If there is no penetration by the added homopolymer, then $a_J = a_{J0}$, a = 1, and $d/d_0 \simeq 1 + \bar{\phi}_h$. The greater the penetration is, the faster the increase in a_J/a_{J0} is, the smaller the value of the coefficient a is, and the slower the increase in d is.

Figures 8 and 9 show this function for the model systems discussed above. Figure 8 is for binary and ternary blends with symmetric copolymers with $Z_{cA} = Z_{cB}$ = 200, and Figure 9 is for the binary and ternary blends with asymmetric copolymers with Z_{cA} = 160 and Z_{cB} = 240. (The ternary blends were on the isopleths.) In all cases a_J/a_{J0} increased with added homopolymers, with the largest increase occurring for smallest Z_h. This implied that the smaller the homopolymer is, the greater is its tendency to penetrate within the copolymers. It was also apparent that for a given copolymer, added solvent had virtually the same effect in binary blends as it did in ternary blends. For blends with symmetric copolymers, Figure 8, a_J/a_{J0}

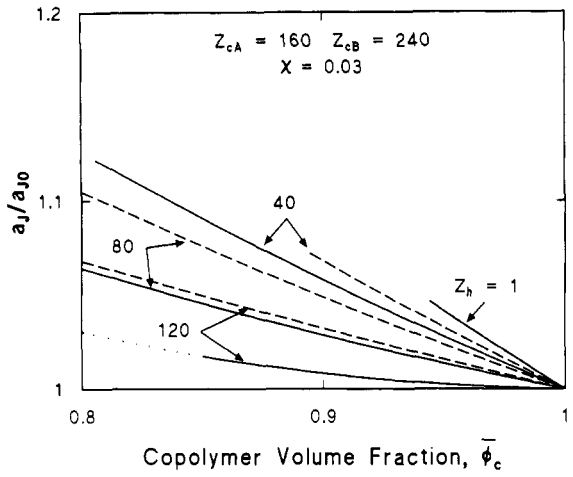

Figure 9. Square root of the average cross-sectional area per copolymer molecule in each interface, a_J, relative to its value for the neat copolymer system, a_{J0}, as a function of $\bar{\phi}_c$ for the systems with asymmetric copolymers. The solid curves correspond to binary blends, as in Figure 4, and the dashed curves correspond to ternary blends on the isopleth as in Figure 6.

was almost the same for binary and ternary blends, being slightly larger in the former. For blends with asymmetric copolymers, Figure 9, the differences were enhnaced and reversed: a_J/a_{J0} was somewhat larger in the ternary blends. For the binary blends, solid lines on each figure, a_J/a_{J0} was smaller for the asymmetric copolymers than for the symmetric ones. This was largely also the case for ternary blends (dashed lines on each figure) except for the larger values of Z_h; at Z_h = 120 they were almost the same.

Figures 10–12 show calculated density profiles which complement the above calculations. Figure 10 is for the binary blends with the symmetric copolymers. The upper panel is for the pure copolymer and illustrates the two profiles $\phi_{cA}(x)$ and $\phi_{cB}(x)$. The second panel in the first column shows the profiles for a blend with 20% homopolymers with Z_h = 40, and beside this are the profiles for a blend with 20% homopolymers but with Z_h = 120. The final panel is for 40% homopolymers with Z_h = 120. A direct comparison of the panels corresponding to $\bar{\phi}_h$ = 0.8 illustrates the greater localization of the homopolymers with the larger degree of polymerization, both between subdomains and within the favorable A subdomain. This localization is even more apparent in the final panel. In this case the maximum of $\phi_{cA}(x)$ has shifted from the center of the A-rich subdomain toward the A–B interface. The degree of this localization depends on both the relative degrees of polymerization and the strength of χ, presumably being enhanced in the strong segregation regime.

Figure 11 is similar to Figure 10, except it is for the asymmetric copolymers, Z_{cA} = 160 and Z_{cB} = 240. The calculations indicated that for this value of χ, an 80/20 blend of these copolymers with homopolymers of Z_h = 40 was not microphase separated, and so we compared the two systems with $\bar{\phi}_c$ = 0.9 instead of $\bar{\phi}_c$ = 0.8 as in Figure 10. Also, the theory predicted that a 60/40 blend with homopolymers with Z_h = 120 macrophase separates,[22] and so we used $\bar{\phi}_c$ = 0.65 for the final panel. The results were qualitatively the same as for the blends with symmetric copolymers but there was a quantitative change. In the case Z_h = 120, the localization of the homopolymer within the subdomain was slightly greater and the local minimum in $\phi_{cA}(x)$ was more pronounced.

Finally, Figure 12 shows density profiles for a ternary blend with the asymmetric copolymers used above and

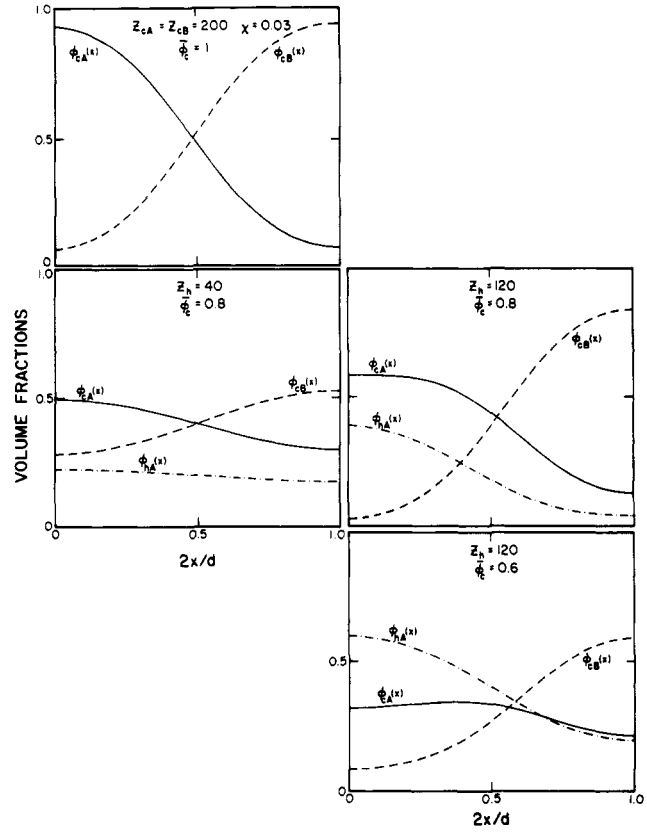

Figure 10. Local volume fractions for binary copolymer/homopolymer blends for different overall volume fractions, $\bar{\phi}_c$, as indicated. The top panel is for symmetric copolymers with Z_{cA} = Z_{cB} = 200. The others are for blends with added A homopolymers for which Z_h = 40, left-hand column, and Z_h = 120, right-hand column. The local volume fractions due to the A and B blocks of the copolymer are labeled $\phi_{cA}(x)$ and $\phi_{cB}(x)$, respectively, and that due to the homopolymers is $\phi_{hA}(x)$.

unequal homopolymer degrees of polymerization. For this case we chose Z_{hA} = 120 = 0.75Z_{cA}, and Z_{hB} = 40 = 0.17Z_{cB}, so that the degree of polymerization of the A homopolymers was almost as large as that of the corresponding copolymer block, whereas the degree of polymerization of the B homopolymers was relatively low. The resulting profiles reflected these choices. The B homopolymers were distributed much more uniformly throughout the full domain than the A homopolymers, which were almost fully expelled from the B subdomains and furthermore were quite localized within the A subdomains. Reflecting this, $\phi_{cB}(x)$ peaked at the center of the B subdomains, but $\phi_{cA}(x)$ had a broad, shallow minimum at the center of the A subdomain, as in the last panels of Figures 10 and 11.

4. Experimental Comparison

We discuss three sets of experiments, beginning with those carried out by Hashimoto et al.[4-6] on PS-*b*-PI/PS and PS-*b*-PI/PS/PI blends. Their copolymers, which they labeled HY8, had a total degree of polymerization of $Z_c \simeq 385$, block degrees of polymerization $Z_{cPS} \simeq 145$ and $Z_{cPI} \simeq 240$, and volume fractions $\bar{\phi}_{cPS} \simeq 0.45$ and $\bar{\phi}_{cPI} \simeq 0.55$. Their homopolymer PS (hPS) had degrees of polymerization $Z_{hPS} \simeq 25$, 40, 100, and 160, and their homopolymer PI (hPI) had $Z_{hPI} \simeq 25$. These were labeled S02, S04, S10, S17, and HI, respectively. Most of the measurements were for binary blends using the hPS, with up to 80% homopolymer. They found that blends with S02, S04, or S10 remained lamellar at $\bar{\phi}_h$ = 0.2 but changed to cylindrical for $\bar{\phi}_h$ = 0.5. However, blends using S17

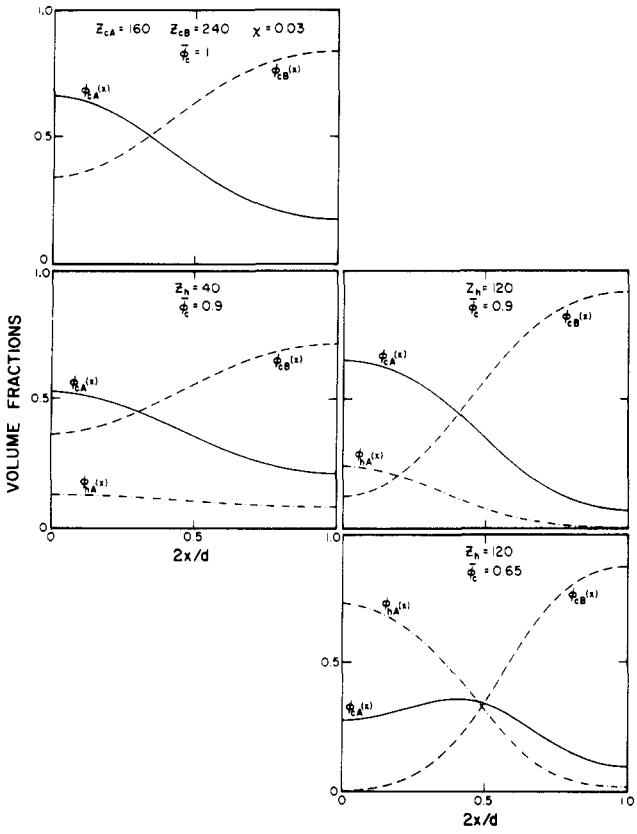

Figure 11. Local volume fractions for binary copolymer/homopolymer blends for different overall volume fractions, $\bar{\phi}_c$, as indicated. The top panel is for asymmetric copolymers with $Z_{cA} = 160$, $Z_{cB} = 240$. The others are for blends with added A homopolymers for which $Z_h = 40$, left-hand column, and $Z_h = 120$, right-hand column. The notation is as in Figure 10.

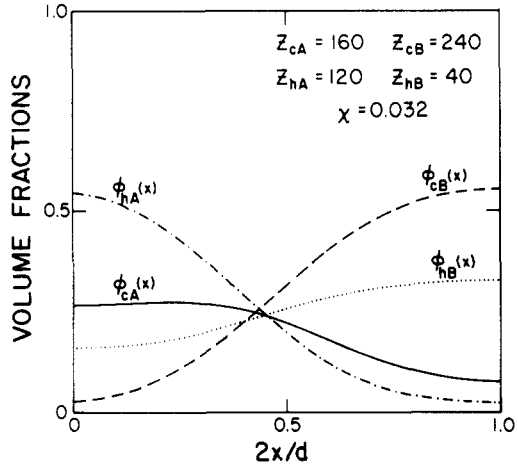

Figure 12. Local volume fractions for a ternary copolymer/homopolymer blend. As indicated, the copolymer is asymmetric, and homopolymers have different degrees of polymerization. The overall copolymer volume fraction is $\bar{\phi}_c = 0.45$, and the overall homopolymer volume fractions are chosen so that the system is on the isopleth, i.e., $\bar{\phi}_{hA}:\bar{\phi}_{hB} = 2:3$.

remained lamellar up to $\bar{\phi}_h = 0.5$. They also studied ternary HY8/S02/HI blends, choosing the overall blend compositions to maintain the system on the isopleth, i.e., $\bar{\phi}_{PS} \simeq 0.45 = 1 - \bar{\phi}_{PI}$. This system maintained a lamellar structure with long-range order for copolymer volume fractions as low as 10%.

Many of their results focused on the domain and subdomain thicknesses d, d_{PS}, and d_{PI}, the average distance between joints in each interface, and the dependence of

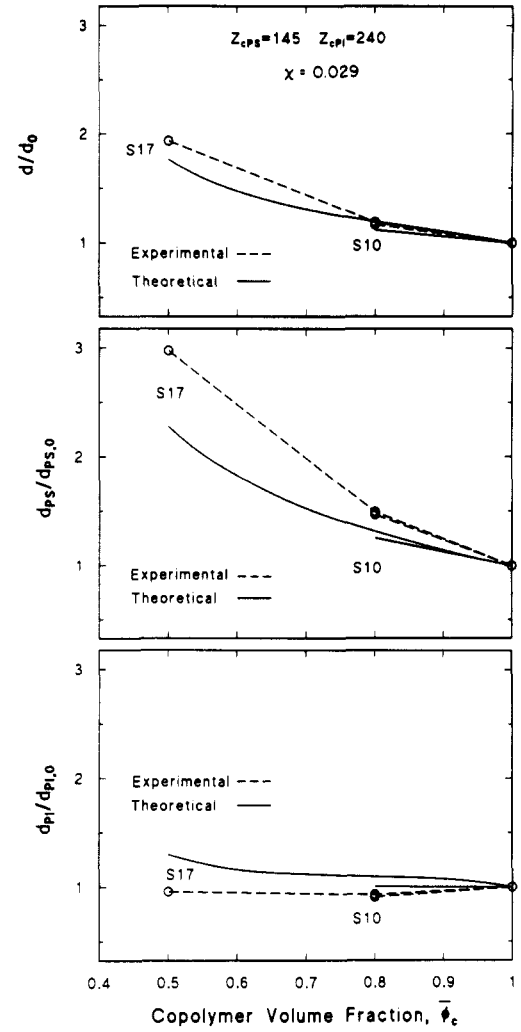

Figure 13. Calculated and measured values of d/d_0, $d_{PS}/d_{PS,0}$ and $d_{PI}/d_{PI,0}$ for PS-*b*-PI/PS blends for copolymers with block degrees of polymerization as shown and for homopolymers with degrees of polymerization $Z_{hPS} = 100$ and 160. These correspond to the HY8/S10 and HY8/S17 blends studied by Hashimoto et al.[4-6] The points are the experimental values, joined by dashed lines intended only as visual guides. The solid curves are the calculated results which were done with a constant value of χ, chosen to be 0.029.

these quantities on composition, degrees of polymerization, and temperature. They also interpreted their results in terms of the localization of the homopolymers within the subdomains. In all cases, their analysis indicated that the systems were in the strong segregation regime and that the solubilized homopolymers were completely segregated into the favorable subdomains.

Some of their data are reproduced in Figures 13 and 14. We summarize those results which relate to the current work as follows:

1. In *binary* systems, the following occurred: (i) at a given temperature T, adding hPS always caused an increase in d and d_{PS} and a decrease in d_{PI} (addition of the S17 initially induced a small decrease in d_{PI}, but this appeared to plateau for $\bar{\phi}_c \lesssim 0.8$); (ii) for a given $\bar{\phi}_{hPS}$, d always decreased with increasing temperature; (iii) the temperature dependence of d strengthened with decreasing Z_{hPS}; and for $Z_{hPS} < Z_{cPS}$, it strengthened with increasing $\bar{\phi}_{hPS}$; (iv) for a given $\bar{\phi}_{hPS}$ and T, d always increased with increasing Z_{hPS}.

2. In *ternary* blends, adding these homopolymers always caused an increase in d, d_{PS}, and d_{PI}.

3. In binary *and* ternary blends, a_J/a_{J0} always increased upon addition of homopolymers, the increase was faster

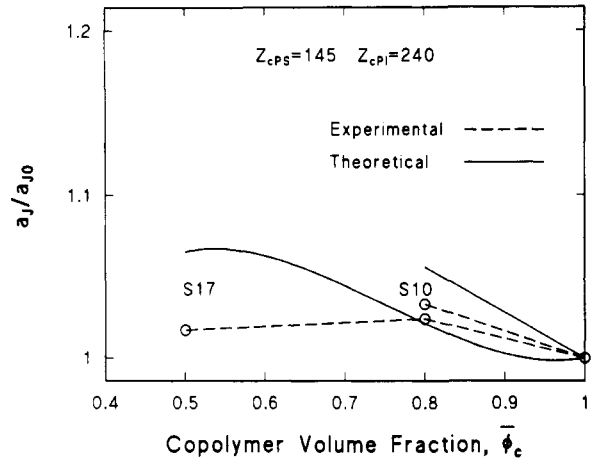

Figure 14. Calculated and measured values of a_J/a_{J0} for the PS-*b*-PI/PS blends of Figure 13. The points are the experimental values, and the solid curves the calculations which were done with a constant value of χ, chosen to be 0.029. The dashed lines joining the experimental points are intended as visual guides.

for small Z_{hPS} than for large Z_{hPS}, and, in general, the variation of a_J/a_{J0} with $\bar{\phi}_c$ was very similar in binary and ternary blends. For blends using S17, the changes in a_J/a_{J0} were small, with an initial increase which was followed by a plateau or slight decrease beyond $\bar{\phi}_c \lesssim 0.8$. These results implied that the low molecular weight homopolymers were solubilized relatively uniformly within the corresponding subdomains, whereas the higher molecular weight homopolymers were more localized within the centers of the subdomains.

4. The effective value of χ was measured in related experiments.[25,26] For these HY8 copolymers, they found $\chi \simeq 0.035$, with the precise value depending on temperature. Adding up to 50% of S02, S04, or S10 homopolymers caused χ to increase by as much as 50%. For a given $\bar{\phi}_{hPS}$, χ increased with decreasing Z_{hPS}. Adding up to 50% of S17 homopolymers caused a decrease in χ of about 10%. The temperature dependence of χ tended to be greater for smaller Z_{hPS}.

In the second set of experiments, Winey and co-workers[7] also used styrene–isoprene copolymers (labeled SI 27/22) with $Z_{cPS} \simeq 255$ and $Z_{cPI} \simeq 325$ and corresponding volume fractions $\bar{\phi}_{cPS} \simeq 0.51$ and $\bar{\phi}_{cPI} \simeq 0.49$. They studied blends with hPS with $Z_{hPS} \simeq 25$, 60, 135, and 355, which they labeled 2.6 hPS, 6 hPS, 14 hPS, and 37 hPS, respectively, using homopolymer weight fractions w_h up to 20% for all cases except 14 hPS, where w_h was as high as 0.24. They estimated a value of $\chi Z_c \simeq 32$, which corresponds to the strong segregation regime. All these blends exhibited the lamellar morphology.

The results in these experiments were more complex than those found by Hashimoto et al.[4-6] The addition of small amounts of either 2.6 hPS or 14 hPS induced small decreases in d, which were followed by increases as additional homopolymers were added. In 90:10 blends with either 6 hPS or 14 hPS, the value of d was virtually the same as for the neat copolymers. All blends with 37 hPS had larger values of d. These results are consistent with the existence of an approximate threshold Z_h^{th}, with a value in the vicinity of $Z_h^{th} \simeq 100 \simeq Z_c/4$. The existence of this apparent threshold contrasts with the results of Hashimoto et al., but this difference may be attributable to molecular weight and composition dependences of χ.

Otherwise, the results agreed qualitatively with those of Hashimoto et al. For a given T and $\bar{\phi}_h$, the domain thickness was an increasing function of Z_{hPS}, and the associated lateral swelling was a decreasing function of Z_{hPS}. The PS subdomain thickness always increased as a function of both Z_{hPS} and $\bar{\phi}_h$. The PI subdomain thickness decreased as hPS was added, except for weight fractions $w_{hPS} \gtrsim 0.2$ for the 14 hPS and $w_{hPS} \gtrsim 0.1$ for the 37 hPS cases. The decrease in d_{PI} was smaller for large Z_{hPS}. The area per chain, i.e., a_J/a_{J0}, decreased or increased as d_{PI} increased or decreased, respectively, and, for the two higher molecular weight homopolymers, it initially increased but then showed a plateau or a decrease for compositions $\bar{\phi}_c \lesssim 0.8$ and $\bar{\phi}_c \lesssim 0.9$ for the 14 hPS and 37 hPS cases, respectively.

Finally, Quan et al.[3] used a series of hydrogenated butadiene homopolymers in a matrix of styrene–hydrogenated butadiene–styrene triblock copolymers, with weight fractions $w_{hPB} = 0.2$. The copolymers had weight fractions $w_{cPS} = 0.49$ and $w_{cPB} = 0.51$ and block degrees of polymerization $Z_{cPB} \simeq 1100$ and $Z_{cPS} \simeq 270$ (each block). They found that the lamellar thickness d decreased for homopolymers with $Z_{hPB} \simeq 200$ and increased for $Z_{hPB} \simeq 600$ and 1100. Their data suggest a threshold value near $Z_{hPB} \simeq 400 \simeq Z_c/4$.

Because all these systems were in the strong segregation regime and also because the last ones involved triblock copolymers, we should not necessarily expect quantitative agreement between the current theoretical calculations and these experiments. Furthermore, the experiments indicated that a full understanding of these systems would require a detailed knowledge of the variation of χ with molecular weights and overall composition, information which is not currently available for these systems in the weak segregation regime. Nonetheless, we can make a qualitative comparison of the predictions for the weak segregation regime with the results of these experiments. A quantitative comparison of calculations for the weak segregation regime with these measurements for the strong segregation regime is also available.[27]

We first compare qualitatively the results of our model calculations with these experiments.

(i) For model binary systems the theory predicted that, for constant χ, the addition of homopolymers with relatively high degrees of polymerization causes an increase in the layer thickness, and the size of the increase is an increasing function of Z_h and $\bar{\phi}_h$. This is consistent with all three sets of experiments. The prediction of a threshold value Z_h^{th} contrasts with the first set of experiments but agrees with the other two. The predicted values of Z_h^{th} are consistent with those suggested by the latter two sets of experiments.

(ii) The theory predicted that d increases with χ. This is consistent with the finding that d always decreased with increasing T.

(iii) The prediction that, for a given $\bar{\phi}_h$, d always increased with Z_h agrees with the experiments for the case $Z_{hPS} < Z_{cPS}$.

(iv) The finding that, for the model systems, a_J/a_{J0} always increased with added homopolymers and that the size of the increase was a decreasing function of Z_h agrees with the experiments, except for those showing plateaus for the higher molecular weight homopolymers. Furthermore, for symmetric copolymers a_J/a_{J0} was virtually the same for binary and ternary blends, as found experimentally.

(v) Expressing the dependence of d on χ as $d \propto \chi^p$, the theory predicted that p increases slightly as both ϕ_h and Z_h increase. This compares with the finding that the temperature dependence of d strengthens with increasing $\bar{\phi}_h$ but decreasing Z_h. This is another case in which a conclusive comparison would require knowing and incor-

porating the full temperature, composition, and molecular weight dependences of χ in the appropriate regime.

In Figures 13 and 14, we show an illustrative set of calculations, for which we chose the copolymer degrees of polymerization of each block to be those used in the experiments, $Z_{cPS} = 145$ and $Z_{cPI} = 240$, and used measured values for the reference densities and Kuhn lengths: $\rho_{0S} = 6.07$ nm^{-3} and $b_S = 0.68$ nm for polystyrene, and $\rho_{0I} = 8.07$ nm^{-3} and $b_I = 0.59$ nm for polyisoprene.[28,29] To stay within the weak segregation regime, we chose $\chi = 0.029$ as in the model calculations of the previous section. This compares with the experimental value of about 0.035 for the copolymers, or a smaller effective, but approximate, value attainable by dilution with DOP. In this context, we did not feel that it was appropriate to include any variation in χ with composition, although it would be straightforward to do so.

The uppermost panel of Figure 13 shows the variation of d/d_0 with composition for two sets of blends, $Z_{hPS} = 100$ and $Z_{hPS} = 160$, corresponding to the experimental blends as indicated on the figure. (With our choice of χ, the theory did not indicate macrophase separation over this concentration range.) For these cases, the measurements indicated little dependence of χ on volume fractions.[25,26] In both cases the layer thickness increased as homopolymers are added, with a faster increase for the $Z_{hPS} = 160$ blend. As indicated, these changes are very similar to those found experimentally in the strong segregation regime. On the other hand, the predictions for the blends using lower molecular weight homopolymers for this regime would differ from the experiments; for constant χ, d/d_0 would decrease as homopolymers are added, which compares with the small increase found experimentally. Furthermore, for the chosen value of χ the MST would soon be reached.

The other panels of Figure 13 compare the calculated values of the subdomain thicknesses with the experimental ones for these systems. The results for these blends were again in qualitative agreement; $d_{PS}/d_{PS,0}$ increased, with the largest increase occurring for the S17 blend, and $d_{PI}/d_{PI,0}$ was nearly constant. However, there were quantitative differences; the increase in $d_{PS}/d_{PS,0}$ in the experiments was larger than that in the calculations, and the small decrease in $d_{PI}/d_{PI,0}$ in the experiments contrasted with the small increase in the calculations.

Figure 14 compares the experimental and theoretical values of a_J/a_{J0} for these two systems. In all cases, its change was on the order of only 5% over the composition ranges studied, with the larger increases occurring for the lower Z_{hPS} blends. In contrast with the calculations for the model systems discussed above, in this case the theory does indicate a nonmonotonic variation of a_J/a_{J0} for the S17 blend, first increasing and then decreasing slightly. The behavior is qualitatively the same as in these experiments and also as in some of those of Winey, as discussed above.

The small increase in a_J/a_{J0} implies a relatively high degree of localization of homopolymer. This is further illustrated in Figure 15, which shows the density profiles for three copolymer volume fractions of HY-8/S17 corresponding to Figures 13 and 14. The first panel represents the calculated density profiles for the pure copolymer. The middle and lower panels, corresponding to $\bar{\phi}_c = 0.9$ and 0.6, illustrate that adding these homopolymers drove the system toward the strong segregation regime, with the amplitudes of the copolymer density variations increasing. Of particular interest is the localization of the homopolymer within the corresponding domain. It was larger here

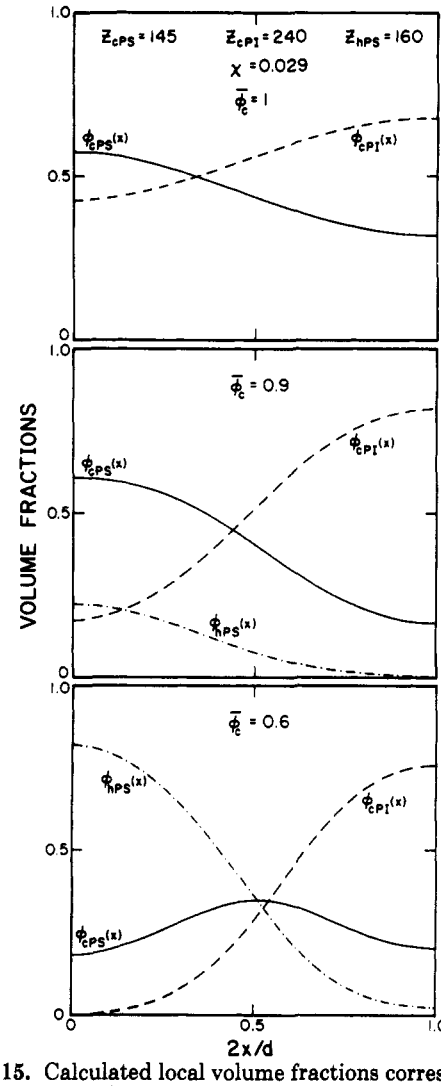

Figure 15. Calculated local volume fractions corresponding to the HY8/S17 blend of Figures 13 and 14 for three compositions as shown and for $\chi = 0.029$.

than in any of the model calculations illustrated in section 3 of this paper, with the local minimum in $\phi_{cPS}(x)$ at the center of the PS subdomain being particularly pronounced in this case.

5. Summary

We have presented an approximate treatment of the lamellar microphase of binary A-*b*-B/A and ternary A-*b*-B/A/B block copolymer/homopolymer blends. Included in the approach was the assumption that there is only one Flory interaction parameter which represents the effective A–B interactions, irrespective of whether the monomers belong to copolymers or homopolymers. It is a mean field theory which makes use of perturbative solutions to the modified diffusion equations for the polymer probability distributions,[19] and its range of validity is restricted to the weak segregation regime. We have, however, included a model for the density profiles which allows for some indication of the effects of composition, χ, and the degrees of polymerization of the homopolymers and each block of the copolymers.

The approach can be considered as an approximation to the full self-consistent mean field theory of such blends. Accordingly, we first compared the results which it gave with full self-consistent calculations for the related problem of A-*b*-B/selective solvent blends, finding that the results of the two calculations agreed very well for values of χ

within about 10% of its value at the MST. For example, expressing the dependence of d on χ as $d \propto \chi^p$, for the series of calculations which we used for the comparison, we found $p = 0.50 \pm 0.01$ (self-consistent calculations) or $p = 0.51 \pm 0.01$ (approximate calculations). This comparison does not, of course, give any information on the validity of mean field theory itself, which neglects fluctuation effects and the swelling effects of good solvent.

Our focus was on the domain thickness d, the two subdomain thicknesses d_A and d_B, the lateral swelling of copolymers by homopolymers as characterized by the average lateral distance between joints, the related localization of the homopolymers, and the density profiles of each component. We carried out model calculations for binary and ternary blends to explore how these quantities depend on the system characteristics, and in section 4 we compared the calculations with three sets of experiments, all of which were in the strong segregation regime. We also carried out a series of calculations for binary styrene–isoprene blends with characteristics similar to those of the experimental systems.

We found that, for constant χ, the addition of homopolymers with relatively high degrees of polymerization, Z_h, caused an increase in the layer thickness, and the size of the increase was an increasing function of Z_h. Homopolymers with relatively small Z_h lead to a decrease in d, and so there was a threshold value Z_h^{th} such that if $Z_h < Z_h^{th}$, then d decreased, but otherwise it increased. The value of Z_h^{th} depended on the total degree of polymerization of the copolymer and the relative degrees of polymerization of each block. For ternary blends, it can depend on the proportions of the added homopolymers. However, in all cases considered, it was on the order of $Z_h^{th} \simeq Z_c/5$. This was comparable to the threshold value for the phenomenon of induced microphase formation. A picture emerged in which added homopolymers with $Z_h \lesssim Z_h^{th}$ tend to destabilize the microphase and reduce the domain thickness, whereas if $Z_h \gtrsim Z_h^{th}$ then they tend to stabilize the microphase and increase d.

The variation in the thickness of each subdomain was more complicated. In binary blends with symmetric copolymers, we found that adding hA homopolymers always induced a lateral swelling of the copolymers, and a consequent reduction in the thickness of the B subdomain. However, the extent of the swelling and the qualitative behavior of d_A depended on the molecular weight of the homopolymers. For very low Z_{hA} the swelling was relatively extensive, and all of d, d_A, and d_B decreased. For intermediate values of Z_{hA}, approximately $Z_h^{th}/2 \lesssim Z_{hA} \lesssim Z_h^{th}$, d and d_B decreased but d_A increased, and for larger Z_{hA}, d and d_A increased while d_B decreased. We also investigated the addition of hA homopolymers to asymmetric copolymers with $Z_{cA} < Z_{cB}$. In these blends, the behavior was more complicated: d_A virtually always increased, but d_B could either increase or decrease. In all these blends in this regime there was another factor as well. If the system approached the MST as homopolymers were added, then both d_A and d_B tended toward $d/2$ in this limit, irrespective of whether they initially increased or decreased.

The behavior of d, d_A, and d_B was qualitatively similar in ternary blends. The quantitative behavior depended on the relative degrees of polymerization and composition.

Following Tanaka et al.,[5] we also expressed our results in terms of the changes in the square root of the average cross-sectional area per copolymer molecule in each layer, a_J/a_{J0}. We found that this almost always increased as homopolymers were added and that the size of the change increased with decreasing Z_h. In calculations explicitly using characteristics of PS and PI, in one case we found nonmonotonic behavior for a_J/a_{J0}; as relatively high molecular weight homopolymers were added, it first increased slightly, reached a broad maximum, and then decreased slightly. This behavior was also found in some experiments. The results are all consistent with the picture that low molecular weight homopolymers are more or less uniformly solubilized in the subdomains but that homopolymers of higher molecular weight are progressively more localized toward the subdomain center. This was illustrated by calculated density profiles in the weak segregation regime. In agreement with experiments, we found that for symmetric copolymers, a_J/a_{J0} was virtually the same for binary and ternary blends.[5]

As discussed in section 4, the predictions for the weak segregation regime were generally consistent with the experimental results for the strong segregation regime. It is possible that those qualitative differences which did appear were due to the differences between the strong and weak segregation regimes or due to variations of χ with the homopolymer and copolymer degrees of polymerization and volume fraction, as well as with temperature.

Acknowledgment. We thank Drs. J. M. Coombes, T. Hashimoto, and J. P. Whitehead for helpful discussions and Mr. J. Vavasour for help with numerical work. This work was supported in part by the Natural Sciences and Engineering Research Council of Canada.

Appendix: Model Density Profiles

To evaluate Δf, and subsequently the four density profiles $\phi_p(x)$, we used a model for $\phi_A(x)$, in particular, the function $u(x;d,\sigma,\tau)$ appearing in eq 26. We expressed u as the convolution of two functions:

$$u(x) = C\int_{-\infty}^{+\infty} dy\, v(x-y)\, w(y) \tag{37}$$

The first function, v, is a periodic step function, chosen to be symmetric about the origin:

$$v(x) = \begin{cases} 1 & \text{for } |x| \le \sigma/2 \\ -\sigma/(d-\sigma) & \text{for } \sigma/2 < |x| \le d \end{cases} \tag{38}$$

This function has zero spatial average, period d corresponding to the lamellar thickness, and subdomain thicknesses σ and $d - \sigma$. The second plateau value, $-\sigma/(d-\sigma)$, is determined by the the relative subdomain thicknesses and the requirement of zero spatial average. The second function, w, is a symmetric, bell-shaped smoothing function:

$$w(x) = \frac{1}{2\tau \cosh^2(x/\tau)} \tag{39}$$

This function has maximum value $w(0) = 1/2\tau$, its width is proportional to τ, and the area under it is unity. Finally, the constant C in eq 37 is chosen so that $u(0) = 1$.

The resultant function, $u(x)$, can be thought of as a smoothed, periodic step function. It can be expressed conveniently as a Fourier series:

$$u(x) = \sum_{n=1}^{\infty} u_n \cos\left(\frac{2\pi n}{d}x\right) \tag{40}$$

with coefficients

$$u_n = 2\pi C \frac{\tau}{(d-\sigma)} \frac{\sin(n\pi\sigma/d)}{\sinh(n\pi^2\tau/d)} \quad (41)$$

In one limit, $\tau/d \gg 1$, the width of the smoothing function is much greater than the period d and, with C chosen appropriately, $u(x)$ becomes a simple cosine function, i.e., the one-wave number form expected for the weak segregation limit.

$$u(x) = \cos\left(\frac{2\pi}{d}x\right) \quad (42)$$

This follows from eq 41; the first Fourier coefficient dominates in this limit. In this case the two subdomain thicknesses are $d_A = d_B = d/2$.

As the width of the smoothing function decreases, then $u(x)$ evolves away from a simple, symmetric cosine function and reflects to a greater degree the underlying step function. Mathematically, the higher order Fourier coefficients grow in importance. In the limit when τ is much less than the width of either plateau in $v(x)$, $u(x)$ consists of two nearly constant regions, joined smoothly by a hyperbolic tangent. For example, a step function of unit height centered at the origin, $v(x) = \theta(x)$, is smoothed to

$$u(x) = {}^1/_2[1 + \tanh(x/\tau)] \quad (43)$$

In this limit, σ and $d - \sigma$ are the subdomain thicknesses d_A and d_B, respectively.

Between these limits, $u(x)$ describes a variety of functions, allowing for a full range of interphase width, which is controlled primarily by τ, and peak values and subdomain thicknesses, which are controlled by d, σ, and τ. In the numerical work of this paper, their values, and hence the profile shapes, were calculated for each blend by minimizing Δf for that blend.

References and Notes

(1) Thomas, E. L.; Alward, D. B.; Kinning, D. L.; Martin, D. L.; Handlin, D. L., Jr.; Fetters, L. J. *Macromolecules* **1986**, *19*, 2197.
(2) Hasegawa, H.; Tanaka, H.; Yamasaki, K.; Hashimoto, T. *Macromolecules* **1987**, *20*, 1651.
(3) Quan, X.; Gancarz, I.; Koberstein, J. T.; Wignall, G. D. *Macromolecules* **1987**, *20*, 1431.
(4) Hashimoto, T.; Tanaka, T.; Hasegawa, H. *Macromolecules* **1990**, *23*, 4378.
(5) Tanaka, H.; Hasegawa, H.; Hashimoto, T. *Macromolecules* **1991**, *24*, 240.
(6) Tanaka, H.; Hashimoto, T. *Macromolecules* **1991**, *24*, 5712.
(7) Winey, K. I. Ph.D. Thesis, University of Massachusetts, 1991.
(8) Helfand, E. In *Recent Advances in Polymer Blends, Grafts and Blocks*; Sperling, L. H., Ed.; Plenum: New York, 1974.
(9) Helfand, E. *Macromolecules* **1975**, *8*, 552.
(10) Helfand, E. *J. Chem. Phys.* **1975**, *62*, 999.
(11) Helfand, E.; Wassermann, Z. R. *Macromolecules* **1976**, *9*, 879.
(12) Helfand, E.; Wassermann, Z. R. *Macromolecules* **1978**, *11*, 960.
(13) Helfand, E.; Wassermann, Z. R. *Macromolecules* **1980**, *13*, 994.
(14) Helfand, E.; Wassermann, Z. R. In *Developments in Block Copolymers*; Goodman, I., Ed.; Elsevier: New York, 1982; Vol. 1.
(15) Leibler, L. *Macromolecules* **1980**, *13*, 1602.
(16) Fredrickson, G. H.; Helfand, E. *J. Chem. Phys.* **1987**, *87*, 697.
(17) Noolandi, J.; Hong, K. M. *Ferroelectrics* **1980**, *30*, 117.
(18) Hong, K. M.; Noolandi, J. *Macromolecules* **1981**, *14*, 727.
(19) Hong, K. M.; Noolandi, J. *Macromolecules* **1983**, *16*, 1083.
(20) Whitmore, M. D.; Noolandi, J. *Macromolecules* **1985**, *18*, 2486.
(21) Whitmore, M. D.; Noolandi, J. *J. Chem. Phys.* **1990**, *93*, 2946.
(22) Banaszak, M.; Whitmore, M. D. *Macromolecules*, in press.
(23) Ohta, T.; Kawasaki, K. *Macromolecules* **1986**, *19*, 2621.
(24) Kruse, R. L. In *Copolymers, Polyblends and Composites*; Platzer, N. A. J., Ed.; American Chemical Society: Washington, DC, 1975; p 141.
(25) Hashimoto, T.; Tanaka, H.; Iizuka, N. In *Space–Time Organization in Macromolecular Fluids, Springer Series in Chemical Physics*; Tanaka, F., Doi, M., Ohta, T., Eds.; Springer-Verlag: Berlin, 1989; Vol. 51.
(26) Tanaka, H.; Hashimoto, T. *Macromolecules* **1991**, *24*, 5398.
(27) Banaszak, M. Ph.D. Thesis, Memorial University of Newfoundland, 1991.
(28) Mori, K.; Tanaka, H.; Hasegawa, H.; Hashimoto, T. *Polymer* **1989**, *30*, 1389.
(29) Brandrup, J.; Immergut, E. H., Eds. *Polymer Handbook*, 2nd ed.; Interscience: New York, 1975.

Registry No. PS, 9003-53-6; (PI)(PS) (copolymer), 105729-79-1.